DisC-Diff: Disentangled Conditional Diffusion Model for Multi-contrast MRI Super-Resolution

Ye Mao[1], Lan Jiang[2], Xi Chen[3], and Chao Li[1,2,4(✉)]

[1] Department of Clinical Neurosciences, University of Cambridge, Cambridge, UK
cl647@cam.ac.uk
[2] School of Science and Engineering, University of Dundee, Dundee, UK
[3] Department of Computer Science, University of Bath, Bath, UK
[4] School of Medicine, University of Dundee, Dundee, UK
https://github.com/Yebulabula/DisC-Diff

Abstract. Multi-contrast magnetic resonance imaging (MRI) is the most common management tool used to characterize neurological disorders based on brain tissue contrasts. However, acquiring high-resolution MRI scans is time-consuming and infeasible under specific conditions. Hence, multi-contrast super-resolution methods have been developed to improve the quality of low-resolution contrasts by leveraging complementary information from multi-contrast MRI. Current deep learning-based super-resolution methods have limitations in estimating restoration uncertainty and avoiding mode collapse. Although the diffusion model has emerged as a promising approach for image enhancement, capturing complex interactions between multiple conditions introduced by multi-contrast MRI super-resolution remains a challenge for clinical applications. In this paper, we propose a disentangled conditional diffusion model, DisC-Diff, for multi-contrast brain MRI super-resolution. It utilizes the sampling-based generation and simple objective function of diffusion models to estimate uncertainty in restorations effectively and ensure a stable optimization process. Moreover, DisC-Diff leverages a disentangled multi-stream network to fully exploit complementary information from multi-contrast MRI, improving model interpretation under multiple conditions of multi-contrast inputs. We validated the effectiveness of DisC-Diff on two datasets: the IXI dataset, which contains 578 normal brains, and a clinical dataset with 316 pathological brains. Our experimental results demonstrate that DisC-Diff outperforms other state-of-the-art methods both quantitatively and visually.

Keywords: Magnetic resonance imaging · Multi-contrast super-resolution · Conditional diffusion model

Y. Mao and L. Jiang—Contribute equally in this work.

H. Greenspan et al. (Eds.): MICCAI 2023, LNCS 14229, pp. 387–397, 2023.
https://doi.org/10.1007/978-3-031-43999-5_37

1 Introduction

Magnetic Resonance Imaging (MRI) is the primary management tool for brain disorders [24–26]. However, high-resolution (HR) MRI with sufficient tissue contrast is not always available in practice due to long acquisition time [19], where low-resolution (LR) MRIs significantly challenge clinical practice.

Super-resolution (SR) techniques promise to enhance the spatial resolution of LR-MRI and restore tissue contrast. Traditional SR methods, e.g., bicubic interpolation [8], iterative deblurring algorithms [7] and dictionary learning-based methods [1] are proposed, which, however, are challenging to restore the high-frequency details of images and sharp edges due to the inability to establish the complex non-linear mapping between HR and LR images. In contrast, deep learning (DL) has outperformed traditional methods, owing to its ability to capture fine details and preserve anatomical structures accurately.

Earlier DL-based SR methods [3,6,13,14,20,23,28] focused on learning the one-to-one mapping between the single-contrast LR MRI and its HR counterpart. However, multi-contrast MRI is often required for diagnosing brain disorders due to the complexity of brain anatomy. Single-contrast methods are limited by their ability to leverage complementary information from multiple MRI contrasts, leading to inferior SR quality. As an improvement, multi-contrast SR methods [5,17,21,22,27] are proposed to improve the restoration of anatomical details by integrating additional contrast information. For instance, Zeng *et al.* designed a CNN consisting of two subnetworks to achieve multi-contrast SR [27]. Lyu *et al.* presented a progressive network to generate realistic HR images from multi-contrast MRIs by minimizing a composite loss of mean-squared-error, adversarial loss, perceptual loss etc. [17]. Feng *et al.* introduced a multi-stage integration network to extract complex interactions among multi-contrast features hierarchically, enhancing multi-contrast feature fusion [5]. Despite these advancements, most multi-contrast methods fail to 1) estimate restoration uncertainty for a robust model; 2) reduce the risk of mode collapse when applying adversarial loss to improve image fidelity.

Conditional diffusion models are a class of deep generative models that have achieved competitive performance in natural image SR [4,10,18]. The model incorporates a Markov chain-based diffusion process along with conditional variables, i.e., LR images, to restore HR images. The stochastic nature of the diffusion model enables the generation of multiple HR images through sampling, enabling inherent uncertainty estimation of super-resolved outputs. Additionally, the objective function of diffusion models is a variant of the variational lower bound that yields stable optimization processes. Given these advantages, conditional diffusion models promise to update MRI SR methods.

However, current diffusion-based SR methods are mainly single-contrast models. Several challenges remain for developing multi-contrast methods: 1) Integrating multi-contrast MRI into diffusion models increases the number of conditions. Traditional methods integrate multiple conditions via concatenation, which may not effectively leverage complementary information in multiple MRI contrasts, resulting in high-redundancy features for SR; 2) The noise and

outliers in MRI can compromise the performance of standard diffusion models that use Mean Squared Error (MSE) loss to estimate the variational lower bound, leading to suboptimal results; 3) Diffusion models are often large-scale, and so are primarily intended for the generation of 2D images, i.e., treating MRI slices separately. Varied anatomical complexity across MRI slices can result in inconsistent diffusion processes, posing a challenge to efficient learning of SR-relevant features.

To address the challenges, we propose a novel conditional disentangled diffusion model (DisC-Diff). To the best of our knowledge, this is the first diffusion-based multi-contrast SR method. The main contribution of our work is fourfold:

- We propose a new backbone network disentangled U-Net for the conditional diffusion model, a U-shape multi-stream network composed of multiple encoders enhanced by disentangled representation learning.
- We present a disentanglement loss function along with a channel attention-based feature fusion module to learn effective and relevant shared and independent representations across MRI contrasts for reconstructing SR images.
- We tailor a Charbonnier loss [2] to overcome the drawbacks of the MSE loss in optimizing the variational lower bound, which could provide a smoother and more robust optimization process.
- For the first time, we introduce an entropy-inspired curriculum learning strategy for training diffusion models, which significantly reduces the impact of varied anatomical complexity on model convergence.

Our extensive experiments on the IXI and in-house clinical datasets demonstrate that our method outperforms other state-of-the-art methods.

2 Methodology

2.1 Overall Architecture

The proposed DisC-Diff is designed based on a conditional diffusion model implemented in [4]. As illustrated in Fig. 1, the method achieves multi-contrast

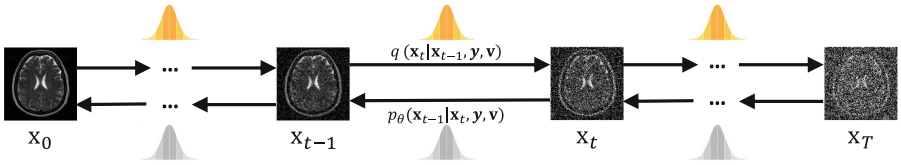

Fig. 1. Conceptual workflow of DisC-Diff on multi-contrast super-resolution. The forward diffusion process q (left-to-right) perturbs HR MRI $\mathbf{x}$ by gradually adding Gaussian noise. The backward diffusion process p (right-to-left) denoises the perturbed MRI, conditioning on its corresponding LR version $\mathbf{y}$ and other available MRI contrasts $\mathbf{v}$.

MRI SR through forward and reverse diffusion processes. Given an HR image $\mathbf{x}_0 \sim q(\mathbf{x}_0)$, the forward process gradually adds Gaussian noise to $\mathbf{x}_0$ over T diffusion steps according to a noise variance schedule $\beta_1, \ldots, \beta_T$. Specifically, each step of the forward diffusion process produces a noisier image $\mathbf{x}_t$ with distribution $q(\mathbf{x}_t \mid \mathbf{x}_{t-1})$, formulated as:

$$q\left(\mathbf{x}_{1:T} \mid \mathbf{x}_0\right) = \prod_{t=1}^{T} q\left(\boldsymbol{x}_t \mid \boldsymbol{x}_{t-1}\right), q\left(\mathbf{x}_t \mid \mathbf{x}_{t-1}\right) = \mathcal{N}\left(\mathbf{x}_t; \sqrt{1-\beta_t}\mathbf{x}_{t-1}, \beta_t \mathbf{I}\right) \quad (1)$$

For sufficiently large T, the perturbed HR $\mathbf{x}_T$ can be considered a close approximation of isotropic Gaussian distribution. On the other hand, the reverse diffusion process p aims to generate a new HR image from $\mathbf{x}_T$. This is achieved by constructing the reverse distribution $p_\theta\left(\mathbf{x}_{t-1} \mid \mathbf{x}_t, \mathbf{y}, \mathbf{v}\right)$, conditioned on its associated LR image $\mathbf{y}$ and MRI contrast $\mathbf{v}$, expressed as follows:

$$\begin{aligned} p_\theta\left(\mathbf{x}_{0:T}\right) &= p_\theta\left(\mathbf{x}_T\right) \prod_{t=1}^{T} p_\theta\left(\mathbf{x}_{t-1} \mid \mathbf{x}_t\right) \\ p_\theta\left(\mathbf{x}_{t-1} \mid \mathbf{x}_t, \mathbf{y}, \mathbf{v}\right) &= \mathcal{N}\left(\mathbf{x}_{t-1}; \boldsymbol{\mu}_\theta\left(\mathbf{x}_t, \mathbf{y}, \mathbf{v}, t\right), \sigma_t^2 \mathbf{I}\right) \end{aligned} \quad (2)$$

where p_θ denotes a parameterized model, θ is its trainable parameters and σ_t^2 can be either fixed to $\prod_{t=0}^{t} \beta_t$ or learned. It is challenging to obtain the reverse distribution via inference; thus, we introduce a disentangled U-Net parameterized model, shown in Fig. 2, which estimates the reverse distribution by learning disentangled multi-contrast MRI representations. Specifically, p_θ learns to conditionally generate HR image by jointly optimizing the proposed disentanglement loss $\mathcal{L}_{\text{disent}}$ and a Charbonnier loss $\mathcal{L}_{\text{charb}}$. Additionally, we leverage a curriculum learning strategy to aid model convergence of learning $\boldsymbol{\mu}_\theta\left(\mathbf{x}_t, \mathbf{y}, \mathbf{v}, t\right)$.

Disentangled U-Net. The proposed Disentangled U-Net is a multi-stream net composed of multiple encoders, separately extracting latent representations.

We first denote the representation captured from the HR-MRI $\mathbf{x}_t$ as $Z_{\mathbf{x}_t} \in \mathbb{R}^{H \times W \times 2C}$, which contains a shared representation $S_{\mathbf{x}_t}$ and an independent representation $I_{\mathbf{x}_t}$ (both with 3D shape $H \times W \times C$) extracted by two 3×3 convolutional filters. The same operations on $\mathbf{y}$ and $\mathbf{v}$ yield $S_{\mathbf{y}}$, $I_{\mathbf{y}}$ and $S_{\mathbf{v}}$, $I_{\mathbf{v}}$, respectively. Effective disentanglement minimizes disparity among shared representations while maximizing that among independent representations. Therefore, $S_{\mathbf{x}_t/\mathbf{y}/\mathbf{v}}$ are as close to each other as possible and can be safely reduced to a single representation S via a weighted sum, followed by the designed Squeeze-and-Excitation (SE) module (Fig. 2 B) that aims to emphasize the most relevant features by dynamically weighting the features in $I_{\mathbf{x}_t/\mathbf{y}/\mathbf{v}}$ or S, resulting in rebalanced disentangled representations $\hat{I}_{\mathbf{x}_t/\mathbf{y}/\mathbf{v}}$ and $\hat{S}$. Each SE module applies global average pooling to each disentangled representation, producing a length-C global descriptor. Two fully-connected layers activated by **SiLU** and **Sigmoid** are then applied to the descriptor to compute a set of weights $\mathbf{s} = [s_1, \ldots, s_i, s_{i+1}, \ldots, s_C]$,

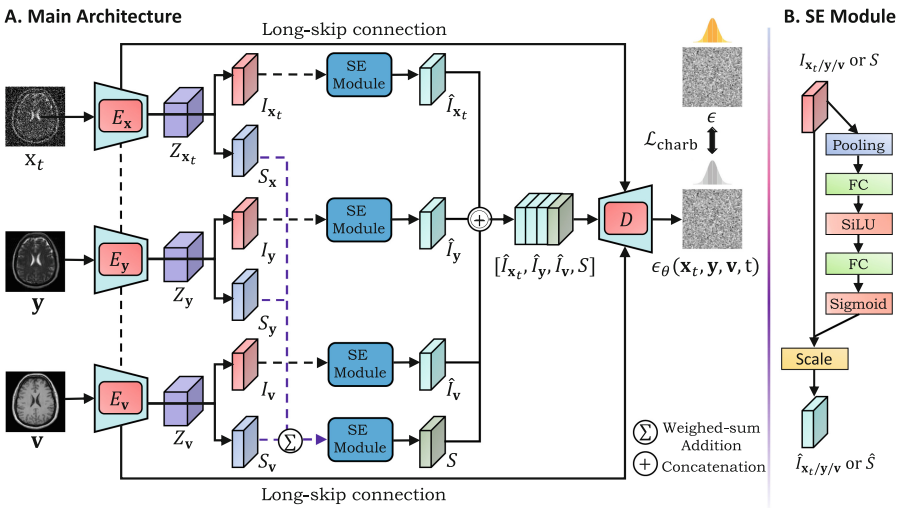

Fig. 2. (A) The disentangled U-Net consists of three encoders processing perturbed HR $\mathbf{x}_t$, LR $\mathbf{y}$, and additional contrast $\mathbf{v}$ respectively. The representations from each encoder are disentangled and concatenated as input to a single decoder D to predict the intermediate noise level $\epsilon_\theta(\mathbf{x}_t, \mathbf{y}, \mathbf{v}, t)$. The architecture includes SE Modules detailed in (B) for dynamically weighting disentangled representations.

where s_i represents the importance of the i-th feature map in the disentangled representation. Finally, the decoder block D shown in Fig. 2 performs upsampling on the concatenated representations $[\hat{I}_{\mathbf{x}_t}, \hat{I}_{\mathbf{y}}, \hat{I}_{\mathbf{v}}, \hat{S}]$ and outputs a noise prediction $\epsilon_\theta(\mathbf{x}_t, \mathbf{y}, \mathbf{v}, t)$ to compute the Gaussian mean in Eq. 3:

$$\boldsymbol{\mu}_\theta\left(\mathbf{x}_t, \mathbf{y}, \mathbf{v}, t\right) = \frac{1}{\sqrt{\alpha_t}}\left(\mathbf{x}_t - \frac{\beta_t}{\sqrt{1-\bar{\alpha}_t}}\boldsymbol{\epsilon}_\theta\left(\mathbf{x}_t, \mathbf{y}, \mathbf{v}, t\right)\right) \tag{3}$$

where $\alpha_t = 1 - \beta_t$ and $\bar{\alpha}_t = \prod_{s=0}^{t} \alpha_s$.

2.2 Design of Loss Functions

To effectively learn disentangled representations with more steady convergence in model training, a novel joint loss is designed in DisC-Diff as follows.

Disentanglement Loss. $\mathcal{L}_{\text{disent}}$ is defined as a ratio between $\mathcal{L}_{\text{shared}}$ and $\mathcal{L}_{\text{indep}}$, where $\mathcal{L}_{\text{shared}}$ measures the $\mathcal{L}_2$ distance between shared representations, and $\mathcal{L}_{\text{indep}}$ is the distance between independent representations:

$$\mathcal{L}_{\text{disent}} = \frac{\mathcal{L}_{\text{shared}}}{\mathcal{L}_{\text{indep}}} = \frac{\|S_{\mathbf{x}_t} - S_{\mathbf{y}}\|_2 + \|S_{\mathbf{x}_t} - S_{\mathbf{v}}\|_2 + \|S_{\mathbf{y}} - S_{\mathbf{v}}\|_2}{\|I_{\mathbf{x}_t} - I_{\mathbf{y}}\|_2 + \|I_{\mathbf{x}_t} - I_{\mathbf{v}}\|_2 + \|I_{\mathbf{y}} - I_{\mathbf{v}}\|_2} \tag{4}$$

Charbonnier Loss. $\mathcal{L}_{\text{charb}}$ is a smoother transition between $\mathcal{L}_1$ and $\mathcal{L}_2$ loss, facilitating more steady and accurate convergence during training [9]. It is less sensitive to the non-Gaussian noise in $\mathbf{x}_t$, $\mathbf{y}$ and $\mathbf{v}$, and encourages sparsity results, preserving sharp edges and details in MRIs. It is defined as:

$$\mathcal{L}_{\text{charb}} = \sqrt{(\epsilon_\theta(\mathbf{x}_t, \mathbf{y}, \mathbf{v}, t) - \epsilon)^2 + \gamma^2)} \tag{5}$$

where γ is a known constant. The total loss is the weighted sum of the above two losses:

$$\mathcal{L}_{\text{total}} = \lambda_1 \mathcal{L}_{\text{disent}} + \lambda_2 \mathcal{L}_{\text{charb}} \tag{6}$$

where λ_1, $\lambda_2 \in (0, 1]$ indicate the weights of the two losses.

2.3 Curriculum Learning

Our curriculum learning strategy improves the disentangled U-Net's performance on MRI data with varying anatomical complexity by gradually increasing the difficulty of training images, facilitating efficient learning of relevant features. All MRI slices are initially ranked based on the complexity estimated by Shannon-entropy values of their ground-truth HR-MRI, denoted as an ordered set $E = \{e_{\min}, \ldots, e_{\max}\}$. Each iteration samples N images whose entropies follow a normal distribution with $e_{\min} < \mu < e_{\max}$. As training progresses, μ gradually increases from $e_{\min}$ to $e_{\max}$, indicating increased complexity of the sampled images. The above strategy is used for the initial M iterations, followed by uniform sampling of all slices.

3 Experiments and Results

Datasets and Baselines. We evaluated our model on the public IXI dataset[1] and an in-house clinical brain MRI dataset. In both datasets, our setting is to utilize HR T1-weighted images HR_{T1} and LR T2-weighted image LR_{T2} created by k-space truncation [3] to restore 2× and 4× HR T2-weighted images, aligning with the setting in [5,22,27].

We split the 578 healthy brain MRIs in the IXI dataset into 500 for training, 6 for validation, and 70 for testing. We apply center cropping to convert each MRI into a new scan comprising 20 slices, each with a resolution 224 × 224. The processed IXI dataset is available for download at this link[2]. The clinical dataset is fully sampled using a 3T Siemens Magnetom Skyra scanner on 316 glioma patients. The imaging protocol is as follows: $\text{TR}_{T1} = 2300$ ms, $\text{TE}_{T1} = 2.98$ ms, $\text{FOV}_{T1} = 256 \times 240\,\text{mm}^2$, $\text{TR}_{T2} = 4840$ ms, $\text{TE}_{T2} = 114$ ms, and $\text{FOV}_{T2} = 220 \times 165\,\text{mm}^2$. The clinical dataset is split patient-wise into train/validation/test sets with a ratio of 7:1:2, and each set is cropped into $\mathbb{R}^{224\times224\times30}$. Both datasets are normalized using the min-max method without prior data augmentations for training.

[1] https://brain-development.org/ixi-dataset/.
[2] https://bit.ly/3yethO4.

We compare our method with three single-contrast SR methods (bicubic interpolation, EDSR [12], SwinIR [11]) and three multi-contrast SR methods (Guided Diffusion [4], MINet [5], MASA-SR [16]) (Table 1).

Table 1. Quantitative results on both datasets with 2× and 4× enlargement scales in terms of mean PSNR (dB) and SSIM. Bold numbers indicate the best results.

Dataset	IXI				Clinical Dataset			
Scale	2×		4×		2×		4×	
Metrics	PSNR	SSIM	PSNR	SSIM	PSNR	SSIM	PSNR	SSIM
Bicubic	32.84	0.9622	26.21	0.8500	34.72	0.9769	27.17	0.8853
EDSR [12]	36.59	0.9865	29.67	0.9350	36.89	0.9880	29.99	0.9373
SwinIR [11]	37.21	0.9856	29.99	0.9360	37.36	0.9868	30.23	0.9394
Guided Diffusion [4]	36.32	0.9815	30.21	0.9512	36.91	0.9802	29.35	0.9326
MINet [5]	36.56	0.9806	30.59	0.9403	37.73	0.9869	31.65	0.9536
MASA-SR [16]	–	–	30.61	0.9417	–	–	31.56	0.9532
DisC-Diff (Ours)	**37.64**	**0.9873**	**31.43**	**0.9551**	**37.77**	**0.9887**	**32.05**	**0.9562**

Implementation Details. DisC-Diff was implemented using PyTorch with the following hyperparameters: $\lambda_1 = \lambda_2 = 1.0$, diffusion steps $T = 1000$, 96 channels in the first layer, 2 BigGAN Residual blocks, and attention module at 28×28, 14×14, and 7×7 resolutions. The model was trained for 200,000 iterations ($M =$ 20,000) on two NVIDIA RTX A5000 24 GB GPUs using the AdamW optimizer with a learning rate of 10^{-4} and a batch size of 8. Following the sampling strategy in [4], DisC-Diff learned the reverse diffusion process variances to generate HR-MRI in only 100 sampling steps. The baseline methods were retrained with their default hyperparameter settings. Guided Diffusion was modified to enable multi-contrast SR by concatenating multi-contrast MRI as input.

Quantitative Comparison. The results show that DisC-Diff outperforms other evaluated methods on both datasets at 2× and 4× enlargement scales. Specifically, on the IXI dataset with 4× scale, DisC-Diff achieves a PSNR increment of 1.44 dB and 0.82 dB and an SSIM increment of 0.0191 and 0.0134 compared to state-of-the-art single-contrast and multi-contrast SR methods [11,16]. The results show that without using disentangled U-Net as the backbone, Guided Diffusion performs much poorer than MINet and MASA-SR on the clinical dataset, indicating its limitation in recovering anatomical details of pathology-bearing brain. Our results suggest that disentangling multiple conditional contrasts could help DisC-Diff accurately control the HR image sampling process. Furthermore, the results indicate that integrating multi-contrast information inappropriately may damage the quality of super-resolved images, as evidenced by multi-contrast methods occasionally performs worse than single-contrast methods, e.g., EDSR showing higher SSIM than MINet on both datasets at 2× enlargement.

Visual Comparison and Uncertainty Estimation. Figure 3 shows the results and error maps for each method under IXI (2×) and Clinical (4×) settings, where less visible texture in the error map indicates better restoration. DisC-Diff outperforms all other methods, producing HR images with sharper edges and finer details, while exhibiting the least visible texture. Multi-contrast SR methods consistently generate higher-quality SR images than single-contrast SR methods, consistent with their higher PSNR and SSIM. Also, the lower variation between different restorations at the 2× scale compared to the 4× scale (Last column in Fig. 3) suggests higher confidence in the 2× restoration results.

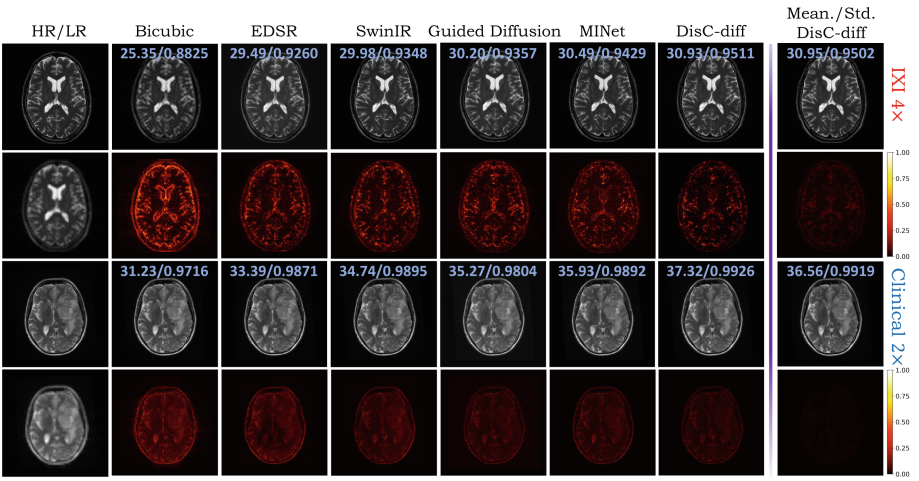

Fig. 3. Visual restoration results and error maps of different methods on IXI (4×) and glioma (2×) datasets, along with mean and standard deviation of our method's sampling results for indicating super-resolution uncertainty (Last column).

Ablation Study. We assess the contribution of three key components in DisC-Diff: 1) $w/o\ \mathcal{L}_{\text{disent}}$ - implement our model without disentanglement loss, 2) $w/o\ \mathcal{L}_{\text{charb}}$ -implement our model using MSE loss instead of charbonnier loss, and 3) w/o curriculum learning - training our model without curriculum learning. The 2× and 4× scale results on the IXI dataset are in Table 2. All three models perform worse than DisC-Diff, indicating that the components can enhance overall performance. The results of $w/o\ \mathcal{L}_{\text{disent}}$ demonstrate that disentangling representations are effective in integrating multi-contrast information. $w/o\ \mathcal{L}_{\text{charb}}$ performs the worst, consistent with our hypothesis that $\mathcal{L}_{\text{MSE}}$ is sensitive to noise in multi-contrast MRI and can cause the model to converge to local optima.

Table 2. Ablation Study on the IXI dataset with 2× and 4× enlargement scale.

Scale	2×		4×	
Metrics	PSNR	SSIM	PSNR	SSIM
$w/o\ \mathcal{L}_{\text{disent}}$	37.15	0.9834	31.08	0.9524
$w/o\ \mathcal{L}_{\text{charb}}$	36.70	0.9846	31.05	0.9532
w/o curriculum learning	37.58	0.9872	31.36	0.9533
DisC-Diff (Ours)	**37.64**	**0.9873**	**31.43**	**0.9551**

4 Conclusion

We present DisC-Diff, a novel disentangled conditional diffusion model for robust multi-contrast MRI super-resolution. While the sampling nature of the diffusion model has the advantage of enabling uncertainty estimation, proper condition sampling is crucial to ensure model accuracy. Therefore, our method leverages a multi-conditional fusion strategy based on representation disentanglement, facilitating a precise and high-quality HR image sampling process. Also, we experimentally incorporate a Charbonnier loss to mitigate the challenge of MRI noise and outliers on model performance. Future efforts will focus on embedding DisC-Diff's diffusion processes into a compact, low-dimensional latent space to optimize memory and training. We plan to integrate advanced strategies (e.g., DPM-Solver++ [15]) for faster image generation and develop a unified model that generalizes across various scales, eliminating iterative training.

References

1. Bhatia, K.K., Price, A.N., Shi, W., Hajnal, J.V., Rueckert, D.: Super-resolution reconstruction of cardiac MRI using coupled dictionary learning. In: 2014 IEEE 11th International Symposium on Biomedical Imaging (ISBI), pp. 947–950. IEEE (2014)
2. Charbonnier, P., Blanc-Feraud, L., Aubert, G., Barlaud, M.: Two deterministic half-quadratic regularization algorithms for computed imaging. In: Proceedings of 1st International Conference on Image Processing, vol. 2, pp. 168–172. IEEE (1994)
3. Chen, Y., Xie, Y., Zhou, Z., Shi, F., Christodoulou, A.G., Li, D.: Brain MRI super resolution using 3d deep densely connected neural networks. In: 2018 IEEE 15th International Symposium on Biomedical Imaging (ISBI 2018), pp. 739–742. IEEE (2018)
4. Dhariwal, P., Nichol, A.: Diffusion models beat GANs on image synthesis. In: Advances in Neural Information Processing Systems, vol. 34, pp. 8780–8794 (2021)
5. Feng, C.-M., Fu, H., Yuan, S., Xu, Y.: Multi-contrast MRI super-resolution via a multi-stage integration network. In: de Bruijne, M., et al. (eds.) MICCAI 2021. LNCS, vol. 12906, pp. 140–149. Springer, Cham (2021). https://doi.org/10.1007/978-3-030-87231-1_14

6. Feng, C.-M., Yan, Y., Fu, H., Chen, L., Xu, Y.: Task transformer network for joint MRI reconstruction and super-resolution. In: de Bruijne, M., et al. (eds.) MICCAI 2021. LNCS, vol. 12906, pp. 307–317. Springer, Cham (2021). https://doi.org/10.1007/978-3-030-87231-1_30
7. Hardie, R.: A fast image super-resolution algorithm using an adaptive wiener filter. IEEE Trans. Image Process. **16**(12), 2953–2964 (2007)
8. Khaledyan, D., Amirany, A., Jafari, K., Moaiyeri, M.H., Khuzani, A.Z., Mashhadi, N.: Low-cost implementation of bilinear and bicubic image interpolation for real-time image super-resolution. In: 2020 IEEE Global Humanitarian Technology Conference (GHTC), pp. 1–5. IEEE (2020)
9. Lai, W.S., Huang, J.B., Ahuja, N., Yang, M.H.: Fast and accurate image super-resolution with deep Laplacian pyramid networks. IEEE Trans. Pattern Anal. Mach. Intell. **41**(11), 2599–2613 (2018)
10. Li, H., et al.: SRDiff: single image super-resolution with diffusion probabilistic models. Neurocomputing **479**, 47–59 (2022)
11. Liang, J., Cao, J., Sun, G., Zhang, K., Van Gool, L., Timofte, R.: SwinIR: image restoration using Swin transformer. In: Proceedings of the IEEE/CVF International Conference on Computer Vision, pp. 1833–1844 (2021)
12. Lim, B., Son, S., Kim, H., Nah, S., Mu Lee, K.: Enhanced deep residual networks for single image super-resolution. In: Proceedings of the IEEE Conference on Computer Vision and Pattern Recognition Workshops, pp. 136–144 (2017)
13. Liu, C., Wu, X., Yu, X., Tang, Y., Zhang, J., Zhou, J.: Fusing multi-scale information in convolution network for MR image super-resolution reconstruction. Biomed. Eng. Online **17**(1), 1–23 (2018)
14. Liu, P., Li, C., Schönlieb, C.-B.: GANReDL: medical image enhancement using a generative adversarial network with real-order derivative induced loss functions. In: Shen, D., et al. (eds.) MICCAI 2019. LNCS, vol. 11766, pp. 110–117. Springer, Cham (2019). https://doi.org/10.1007/978-3-030-32248-9_13
15. Lu, C., Zhou, Y., Bao, F., Chen, J., Li, C., Zhu, J.: DPM-solver++: fast solver for guided sampling of diffusion probabilistic models. arXiv preprint: arXiv:2211.01095 (2022)
16. Lu, L., Li, W., Tao, X., Lu, J., Jia, J.: MASA-SR: matching acceleration and spatial adaptation for reference-based image super-resolution. In: Proceedings of the IEEE/CVF Conference on Computer Vision and Pattern Recognition, pp. 6368–6377 (2021)
17. Lyu, Q., et al.: Multi-contrast super-resolution MRI through a progressive network. IEEE Trans. Med. Imaging **39**(9), 2738–2749 (2020)
18. Rombach, R., Blattmann, A., Lorenz, D., Esser, P., Ommer, B.: High-resolution image synthesis with latent diffusion models. In: Proceedings of the IEEE/CVF Conference on Computer Vision and Pattern Recognition, pp. 10684–10695 (2022)
19. Shi, F., Cheng, J., Wang, L., Yap, P.T., Shen, D.: LRTV: MR image super-resolution with low-rank and total variation regularizations. IEEE Trans. Med. Imaging **34**(12), 2459–2466 (2015)
20. Shi, J., Liu, Q., Wang, C., Zhang, Q., Ying, S., Xu, H.: Super-resolution reconstruction of MR image with a novel residual learning network algorithm. Phys. Med. Biol. **63**(8), 085011 (2018)
21. Stimpel, B., Syben, C., Schirrmacher, F., Hoelter, P., Dörfler, A., Maier, A.: Multi-modal super-resolution with deep guided filtering. In: Bildverarbeitung für die Medizin 2019. I, pp. 110–115. Springer, Wiesbaden (2019). https://doi.org/10.1007/978-3-658-25326-4_25

22. Tsiligianni, E., Zerva, M., Marivani, I., Deligiannis, N., Kondi, L.: Interpretable deep learning for multimodal super-resolution of medical images. In: de Bruijne, M., et al. (eds.) MICCAI 2021. LNCS, vol. 12906, pp. 421–429. Springer, Cham (2021). https://doi.org/10.1007/978-3-030-87231-1_41
23. Wang, J., Chen, Y., Wu, Y., Shi, J., Gee, J.: Enhanced generative adversarial network for 3D brain MRI super-resolution. In: Proceedings of the IEEE/CVF Winter Conference on Applications of Computer Vision, pp. 3627–3636 (2020)
24. Wei, Y., et al.: Multi-modal learning for predicting the genotype of glioma. IEEE Trans. Med. Imaging (2023)
25. Wei, Y., et al.: Structural connectome quantifies tumour invasion and predicts survival in glioblastoma patients. Brain **146**, 1714–1727 (2022)
26. Wei, Y., Li, C., Price, S.J.: Quantifying structural connectivity in brain tumor patients. In: de Bruijne, M., et al. (eds.) MICCAI 2021. LNCS, vol. 12907, pp. 519–529. Springer, Cham (2021). https://doi.org/10.1007/978-3-030-87234-2_49
27. Zeng, K., Zheng, H., Cai, C., Yang, Y., Zhang, K., Chen, Z.: Simultaneous single- and multi-contrast super-resolution for brain MRI images based on a convolutional neural network. Comput. Biol. Med. **99**, 133–141 (2018)
28. Zhang, Y., Li, K., Li, K., Fu, Y.: MR image super-resolution with squeeze and excitation reasoning attention network. In: Proceedings of the IEEE/CVF Conference on Computer Vision and Pattern Recognition, pp. 13425–13434 (2021)